Microstructural differences between naturally-deposited and laboratory beach sands

Amy Ferrick,[1,*] Vanshan Wright,[2,3] Michael Manga,[1] and Nicholas Sitar[4]

[1]*University of California Berkeley, Department of Earth and Planetary Science, Berkeley, California, USA, 94720*
[2]*Woods Hole Oceanographic Institution, Geology and Geophysics Department, Woods Hole, Massachusetts, USA, 02543*
[3]*University of California San Diego, Scripps Institution of Oceanography, La Jolla, California, USA, 92037*
[4]*University of California Berkeley, Department of Civil and Environmental Engineering, Berkeley, California, USA, 94720*

The orientation of and contacts between grains of sand reflect the processes that deposit the sands. Grain orientation and contact geometry also influence mechanical properties. Quantifying and understanding sand microstructure thus provide an opportunity to understand depositional processes better and connect microstructure and macroscopic properties. We compare naturally-deposited beach sands with laboratory sands created by pouring grains into a container (a process called pluviation). We find that naturally-deposited sands have a narrower distribution of coordination number (i.e., the number of touching grains) and a broader distribution of grain orientations than pluviated sands. We explain the differences through particle rearrangement by flowing water on beaches, which repositions and reorients grains that initially had unstable configurations.

I. INTRODUCTION

Sand depos its are formed by accumulation of individual grains. The transporting medium and sedimentary environment will influence sands' microstructure, including the porosity, coordination number (i.e., the number of contacts between grains), spatial organization, and orientation of grains. These microstructural properties influence macroscopic properties of sands, including elastic properties and hence seismic velocities [1-3], strength and particle breakage [4,5], and liquefaction susceptibility [6,7]. Thus, microstructure presumably explains behavioral differences of sands deposited differently [8-10].

Experimental measurements of sands' physical properties typically rely on samples reconstructed using different methods of sample preparation such as wet and dry tamping, and wet and dry pluviation [11]. However, it has been well documented that reconstituted sands' mechanical properties are a function of the sample preparation method and, therefore, they do not necessarily behave the same as in situ sands [12]. Since the processes depositing the particles in natural deposition and pluviation are different, the microstructure and physical properties differ as well [13]. In pluviated sands, particles preferentially orient in the horizontal plane and symmetrically distribute around the vertical axis [14]. Sands deposited in nature generally develop orientations parallel to the moving medium's direction (e.g., ocean water), although beach sands have more complicated orientations because the direction and magnitude of waves, swash, and backwash vary over time [15]. Despite different depositional processes, the average coordination number of pluviated sands is similar to that of naturally-deposited sands with the same porosity [16].

However, depositional processes may influence the stability of contacts [17], which is determined by the relative sizes and positions of touching grains. A better understanding of how depositional methods influence these microstructural characteristics is needed to explain differences in behavior exhibited by sands deposited differently.

Here, we investigate the effect of depositional history by comparing the microstructures of pluviated and naturally-deposited samples of the same sand. We use x-ray computed microtomography to reconstruct 3-D volumes of pluviated and naturally-deposited beach sand from Alameda County, California. We use image analysis techniques to quantify microstructural properties, including porosity, coordination number, and grain orientation. We find that the distributions of microstructural properties differ for the two depositional methods. Our objective is to understand how naturally-deposited beach sands differ from reconstituted beach sands in order to better understand depositional processes.

II. METHODS

To compare the microstructures of natural beaches and pluviated sands, we first collected sand cores from a natural beach. We then pluviated a sample with sand from the same beach. We acquired three-dimensional x-ray computed microtomographic images of the samples. Image analyses, followed by statistical analyses, allowed us to quantify and compare the microstructures of the sands deposited by the two deposition methods.

A. Sample Collection

We collected three undisturbed samples of naturally-deposited sand from an unnamed beach (Supplementary

---

Figure S1 [18]) in Alameda County, California, USA (37°51'04'' N, 122°18'00'' W). Collection took place at low tide, approximately 7 m from the waterline, and at depths of 1 cm, 6 cm, and 11 cm. We collected the samples by gently inserting a transparent plastic straw into the sand at each depth. The straws are 11 mm in diameter and 22 mm in length. Then, we removed the sand around the outside of the straw before gently removing the straw. Before transporting the straws, we temporarily sealed the straws with tape and wrapped the straws in paper towels. To ensure preservation of the samples, we then covered each end of the samples with cheesecloth and enclosed the entire straw with melted wax.

To create the pluviated sample, we poured sand from the Alameda County collection site through a funnel held 30 cm above a plastic straw. We chose this height to achieve a similar porosity to that of the naturally-deposited samples [11]. We sealed the pluviated sample with cheesecloth and wax in a similar fashion.

B. XRCT Imaging

We acquired x-ray computed microtomography images of each sample on beamline 8.3.2 at the Advanced Light Source, Lawrence Berkeley National Lab. We imaged using 30 keV monochromatic x-rays, a 200-millisecond exposure time, and collected 1969 projections during continuous sample rotation through 180°. Each image volume comprises ~500 two-dimensional image slices. We captured the images using a PCO edge camera, a 1X Nikon lens, and a 50 mm LuAG scintillator. The linear dimension of each voxel is 6.45 μm. We used Xi-cam software for image reconstruction [19], including center of rotation optimizations, ring removal, and outlier removal.

C. Image Analyses

Image analyses allowed us to identify individual grains and quantify their properties. We first binarized the images (i.e., separated each voxel into the 'grain' phase or 'pore' phase) using ImageJ's machine learning algorithm, Trainable Weka Segmentation [20]. We trained the classifier with approximately five manually segmented grains and pores on every 50th image in the image volume representing each sample. We tested various training features and found Gaussian blur the most effective. The algorithm trains the classifier on the original images and blurred versions, each with a different Gaussian sigma value (minimum sigma = 1, maximum sigma = 8). We manually inspected the binarization accuracy by comparing the binarized image volume with the original image volume. We then segmented and labeled each grain using the Distance Transform Watershed 3D algorithm. Here, we tested different

parameters and found the most effective to be the Borgefors distance map with a dynamic parameter of 2 and a connectivity parameter of 6. The distance map influences location and shape of object borders, the dynamic parameter influences degree of segmentation, and the connectivity influences object roundness. The algorithm removes one pixel-wide gap between touching grains, so we applied a morphological closing filter to reestablish contacts. To quantify uncertainty in the segmentation process, we performed this process on a 15-image subset of one of the samples 15 times. We used Software for Practical Analysis
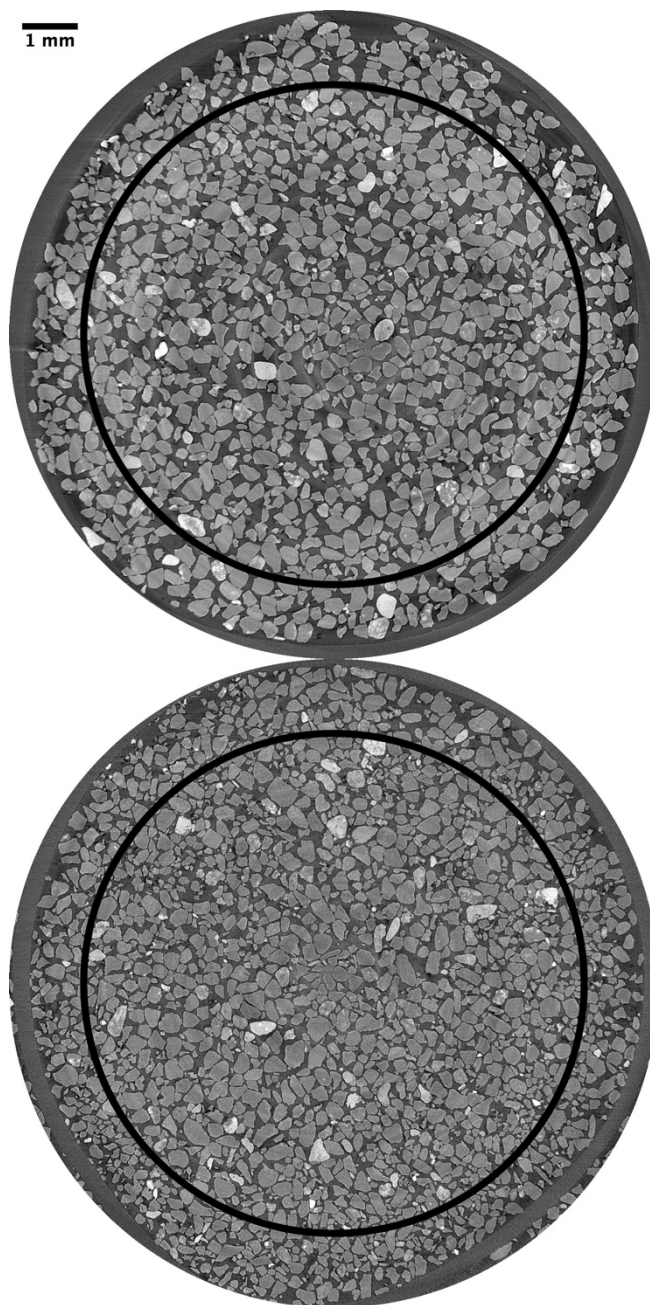

1 mm

FIG. 1. X-ray computed microtomography images showing horizontal cross-sections of the naturally-deposited (top) and pluviated (bottom) sands. The black circles denote the 9 mm radius of the image subsection we consider in our analyses.
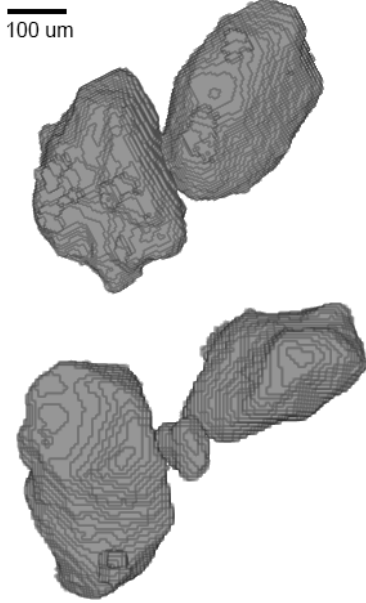
FIG. 2. 3D rendering of a stable contact configuration (top) and an unstable contact configuration (bottom).

of Materials [21] to quantify each sample's microstructural properties, including porosity, grain orientation, and coordination number. To quantify geometric anisotropy, we used a scalar anisotropy factor defined as

$$ a = \frac{15}{2}\sqrt{\frac{3}{2}}R'_{ij} \qquad (2.1) $$

where R'_{ij} is the deviatoric part of the grain orientations' fabric tensor [22]. Finally, we performed a t-test and a Kolmogorov-Smirnov test to compare microstructural properties' distributions for the two depositional methods.

III. RESULTS

We find that (1) x-ray computed microtomography data retain the microstructures of the sands, (2) grain and pore properties can be reliably compared for images of the same resolution, and (3) the distributions of coordination numbers and grain orientations in pluviated and naturally-deposited sands differ.

A. Uncertainty and Resolution

The x-ray microtomography data capture the microstructural properties of the sands. Grain and pore distributions appear consistent within the inner 9 mm of each sample (Fig. 1). Some anomalously large pores exist within 1 mm of the sample walls, suggesting that the microstructure was disturbed immediately adjacent to the sampling tube. Thus, we only analyze the innermost 9 mm of the samples.

Our segmentation procedure is reliable. When we segment a 15-image subset 15 different times, the estimated porosities differ by 2%. Repeating the segmentation process on an entire sample 3 different times results in 3.4% porosity variation, 6.9% mean coordination number variation, and 8.2% mean grain surface area variation. Thus, differences in results introduced by the segmentation procedures are relatively small.

We can make a meaningful comparison between the x-ray microtomography images of pluviated and naturally-deposited sands. The images exhibit similar levels of resolution, noise, and blur (Fig. 1). Further, the segmented image volumes capture grain contacts at a high resolution (Fig. 2). Because images of finite resolution produce systematic, resolution-dependent overdetection of grain contacts [23], scanning all samples at the same resolution allows us to compare distributions of coordination number. To quantify overdetection of contacts, we generate 3-D images of spheres, for which exact size, position, and contact relationships are known, at varying resolutions. We define resolution as voxel size compared to grain diameter. Overdetection of contacts decreases with increasing resolution, and contacts are approximately 40% overdetected at the resolution of the beach sand samples (Supplementary Fig. S2 [18]). However, this is likely an upper bound for contact overdetection in the images of real sands. Whereas the artificially generated images are defined to include instances of nearly contacting spheres, any two grains in the images of real sands close enough to appear contacting likely are indeed in contact.

B. Pluviated and Naturally-Deposited Microstructures

The pluviated and naturally-deposited sands exhibit distinct microstructures (Table I). The porosities of the naturally-deposited samples are 0.40, 0.37, and 0.37 from shallowest to deepest samples. The porosity of the pluviated sample is 0.38. Mean coordination number is lower in the pluviated sands (7.45) than in the naturally-deposited sands (8.15, 7.71, and 8.31 from shallowest to deepest). Standard deviation for coordination number in the pluviated sands (3.66) is higher than the naturally-deposited sands (3.36, 3.01, and 3.36 from shallowest to deepest). T-test and Kolmogorov-Smirnov tests reveal that the means and distributions of coordination number in the naturally-deposited and pluviated samples are different (Table II). Coordination numbers in all samples range from 2 to 20 (Fig. 3). The naturally-deposited sands have a lower frequency of grains with low coordination numbers (<5) and a lower frequency of grains with high coordination numbers (>14) than the pluviated sands (Fig. 3). Preferred orientation of the

TABLE I. Properties of the sands

Deposition	Depth (cm)	Porosity	Mean coordination number (± 1σ)	Scalar anisotropy factor
Natural	0	0.403	8.15 ± 3.64	0.38
Natural	6	0.374	7.71 ± 3.01	0.34
Natural	11	0.371	8.31 ± 3.36	0.41
Pluviated	n/a	0.385	7.45 ± 3.64	0.53

TABLE II. Results of T-test and Kolmogorov-Smirnov test. 'DF' indicates degrees of freedom.

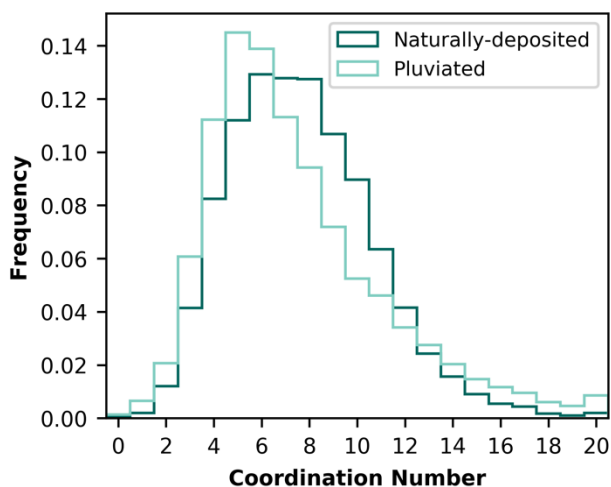| Test	Coordination Number			Long axis elevation angle		
	Score	P-value	DF	Score	P-value	DF
T	7.25	4.24E-13	36622	13.52	1.48E-40	72128
K-S	0.11	2.09E-80	36622	0.051	4.17E-36	72128

FIG. 3. Distribution of coordination number for naturally-deposited and pluviated samples.

pluviated sands lies in the horizontal plane, while preferred orientations of the naturally-deposited sands lie at angles of 0 to 60 from the horizontal (Figs. 4, 5). The preferred orientation in the horizontal plane has a range of approximately 180 degrees in the naturally-deposited samples (Fig. 5). The pluviated sands exhibit a higher degree of geometrical anisotropy than the naturally-deposited sands (Table I). T-tests and Kolmogorov-Smirnov tests show that the orientation distribution of naturally-deposited and pluviated samples are different (Table II).

IV. DISCUSSION

We identify two primary differences between natural and pluviated sands: (1) naturally-deposited sands have a lower frequency of grains with very low (<5) and very high (>20) coordination numbers, and (2) naturally-deposited sands, unlike pluviated sands, have an inclined preferred grain orientation. We now argue that perturbations from flowing water at beaches can explain these microstructural differences.

A. Coordination Number

Differences in coordination numbers can be explained by the effects of flowing water in naturally-deposited beach sands. Flowing water, such as swash and backwash on a beach, preferentially mobilizes small grains [24]. We propose that mobilization of small grains hinders formation of unstable contacts and destabilizes any transient, unstable contacts that form. Here, unstable contact configurations refer to two large grains fully separated by a small grain wedged between them (Fig. 2) [17]. Stable contact configurations refer to two large grains in direct contact (Fig. 2). Small grains wedged between large grains may be mobilized by flowing water, thus allowing for small grains to find configurations with a higher number of contacts. We argue that this process leads to a depletion in low coordination numbers observed in naturally-deposited sands
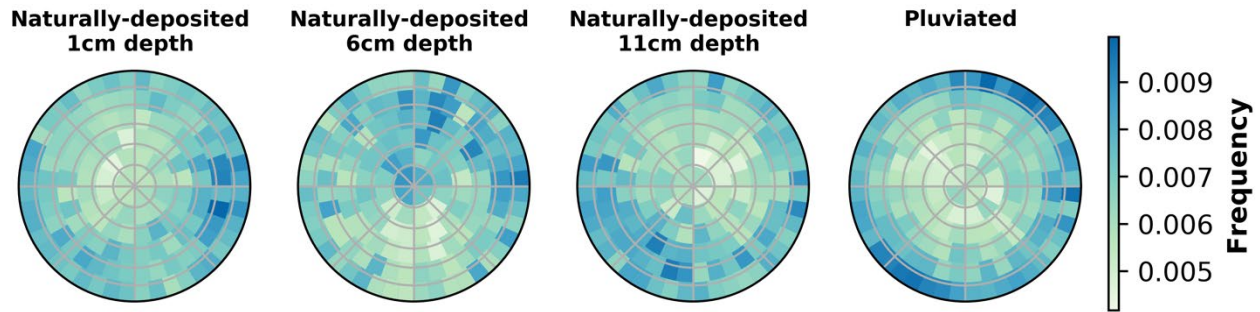
FIG. 4. Distributions of grain long axis orientation on an equal-area projection. Circular grid lines are at increments of 15°.
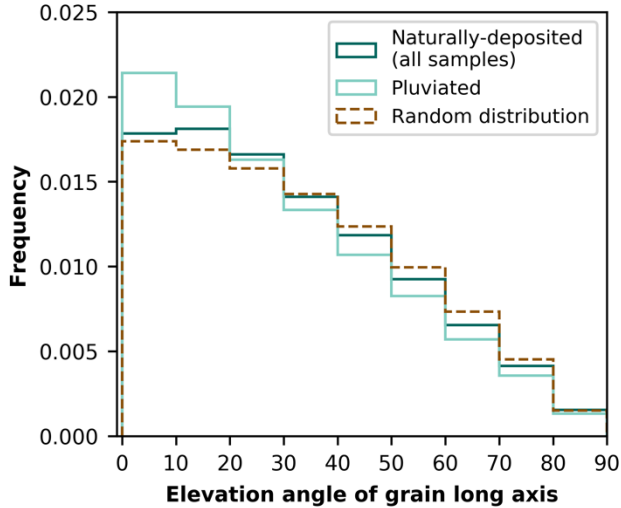

FIG. 5. Distributions of plunge of grain long axis.

compared with pluviated sands (Fig. 3). When a small grain is removed from its wedged position between two large grains, the large grains can contact each other. Contact with a large grain occupies more surface area than contact with a small grain (see Fig. 2). As a result, the two touching large grains each have less surface area to contact smaller grains. Thus, improvement in contact stability can explain the depletion in very high coordination numbers observed in naturally-deposited sands (Fig. 3). This interpretation is consistent with existing studies that found that sand columns created by air pluviation have a higher number of unstable contacts than sands formed by water sedimentation (e.g., Ref. [17]). These studies, while able to manually identify and count unstable and stable contacts, consider fewer grains and do not constrain microstructure using x-ray microtomography.

B. Grain Orientation

Two different depositional processes may explain the differences in preferred spatial orientations of the sand grains. The horizontal preferred orientation of the long axis of the pluviated sand grains is consistent with existing studies of laboratory sands, which find that grains align normal to the direction of pouring [14,25]. However, we find that the pluviated sand grains are not distributed symmetrically around the vertical axis (Fig. 4). We propose that the orientation of newly deposited grains influences the orientation of subsequently deposited grains. Thus, if enough of the initially deposited grains randomly align azimuthally, the subsequently deposited grains follow suit.

As sample collection only preserves the core's vertical direction, and not its azimuthal orientation, the preferred azimuth direction of the naturally-deposited sands is unknown. However, grains generally develop preferred orientations parallel to the flow direction [15]. The large range of the preferred azimuth (>90 degrees) could arise from different swash and backwash flow directions. The preferred inclination of the naturally-deposited sands is not horizontal, unlike the pluviated sample, even though flow was horizontal (beach slope was <2 degrees). Instead, the naturally-deposited sands have inclinations between 0 and 60 degrees from the horizontal (Figs. 4, 5). We propose that beach sands are originally deposited with a horizontal orientation, but this horizontality is quickly disturbed by swash action. The preferred orientation is reminiscent of the imbrication seen in larger grains in deposits from rivers [26,27], submarine sediment flows that form turbidites [28,29], and some volcanic particle-laden flows [30], though here preserved in sand-size particles. Imbrication is attributed to bedload transport wherein particles roll over a surface [31]. In contrast, pluviation does not introduce repeated disturbances, which can explain how a strong geometric anisotropy (i.e., preferred horizontality) is retained in the pluviated sand grains.

V. CONCLUSION

Naturally-deposited sands have a lower frequency of both very low coordination numbers and very high coordination numbers. The pluviated sands exhibit a strong horizontal preferred orientation, while the naturally-deposited sands exhibit an imbricated preferred orientation. We propose that flowing water at beaches (e.g., waves, swash, and backwash) remobilizes and reorients sand grains, resulting in fewer

unstable grain contacts and a lower degree of geometric anisotropy in naturally-deposited sands than their pluviated counterparts.

ACKNOWLEDGEMENTS

---

[1] F. Gassmann, Elasticity of porous media. Vierteljahrsschr. Naturforsch. Ges. **96**, 1 (1951).

[2] M. A. Zimmer, M. Prasad, G. Mavko, and A. Nur, Seismic velocities of unconsolidated sands: Part 1— Pressure trends from 0.1 to 20 MPa, Geophysics **72**, E1 (2007).

[3] A. Muqtadir, S. Al-Dughaimi, M. E. Kandil, A. Ali, and J. P. Dvorkin, Elastic and mechanical properties of dune sand: Experiments and models, J. Geophys. Res-Sol. Ea. **124**, 7978 (2019).

[4] Z. Karatza, E. Andò, S. A. Papanicolopulos, G. Viggiani, and J. Y. Ooi, Effect of particle morphology and contacts on particle breakage in a granular assembly studied using X-ray tomography, Granul. Matter **21**, 1 (2019).

[5] R. C. Hurley, J. Lind, D. C. Pagan, M. A. Homel, M. C. Akin, and E. B. Herbold, Linking initial microstructure and local response during quasistatic granular compaction, Phys. Rev. E **96**, 012905 (2017).

[6] B. Ye, H. Hu, X. Bao, and P. Lu, (2018). Reliquefaction behavior of sand and its mesoscopic mechanism, Soil Dyn. Earthq. Eng. **114**, 12 (2008).

[7] M. Oda, K. Kawamoto, K. Suzuki, H. Fujimori, and M. Sato, Microstructural interpretation on reliquefaction of saturated granular soils under cyclic loading, J. Geotech. Geoenviron. Eng. **127**, 416 (2001).

[8] S. Miura and S. Toki, A sample preparation method and its effect on static and cyclic deformation-strength properties of sand, Soils Found. **22**, 61 (1982).

[9] R. S. Ladd, Specimen preparation and liquefaction of sands, J. Geotech. Eng.-ASCE **100**, 1180-1184 (1974).

[10] J. P. Mulilis, H. B. Seed, C. K. Chan, J. K. Mitchell, and K. Arulanandan, Effects of sample preparation on sand liquefaction, J. Geotech. Eng.-ASCE **103**, 91-108 (1977).

[11] M. E. Raghunandan, A. Juneja, and B. C. Benson Hsiung, Preparation of reconstituted sand samples in the laboratory, Int. J. Geotech. Eng. **6**, 125-131 (2012).

[12] Y. P. Vaid and S. Sivathayalan, Fundamental factors affecting liquefaction susceptibility of sands, Can. Geotech. J. **37**, 592 (2000).

[13] N. Sitar, F. E. Garcia, E. Ando, G. Viggiani, Characterization of the depositional fabric and stress-strain behavior of estuarine sand bar deposits from the San Francisco Bay using 3-D x-ray computed tomography (3-D XRCT), AGU Fall Meeting Abstracts, EP51B-10 (2019).

[14] A. K. Parkin, C. M. Gerrard, and D. R. Willoughby, Discussion on Deformation of sand in shear, J. Soil Mech. Found. Div. **94**, 336 (1968).

[15] C. E. Johansson, Structural studies of sedimentary deposits, Geol. Fören. Stock. För. **87**, 3 (1965).

[16] V. Wright, A. Ferrick, and M. Manga, Coordination numbers in natural beach sand, EPJ Web of Conferences (in preprint).

[17] J. A. Yamamuro, F. M. Wood, and P. V. Lade, Effect of depositional method on the microstructure of silty sand, Can. Geotech. J. **45**, 1538 (2008).

[18] See Supplementary Material at [URL will be inserted by publisher] for image of sample collection, extended table of results, and investigation of the effect of image resolution.

[19] R. J. Pandolfi, D. B. Allan, E. Arenholz, L. Barroso-Luque, S. I. Campbell, T. A. Caswell, A. Blair, F. De Carlo, S. Fackler, A. P. Fournier, G. and Freychet, Xi-cam: a versatile interface for data visualization and analysis, J. Synchrotron Radiat. **25**, 1261 (2018).

[20] I. Arganda-Carreras, V. Kaynig, C. Rueden, K. W. Eliceiri, J. Schindelin, A. Cardona, and H. Sebastian Seung, Trainable Weka Segmentation: a machine learning tool for microscopy pixel classification, Bioinformatics **33**, 2424 (2017).

[21] O. Stamati, E. Andò, E. Roubin, R. Cailletaud, M. Wiebicke, G. Pinzon, C. Couture, R. C. Hurley, R. Caulk, D. Caillerie, and T. Matsushima, spam: Software for Practical Analysis of Materials, J. Open Source Softw. **5**, 2286 (2020).

[22] X. Gu, J. Hu, and M. Huang, Anisotropy of elasticity and fabric of granular soils, Granul. Matter **19**, 33 (2017).

[23] M. Wiebicke, E. Andò, I. Herle, and G. Viggiani, On the metrology of interparticle contacts in sand from x-ray tomography images, Meas. Sci. Technol. **28**, 124007 (2017).

[24] P. McLaren and D. Bowles, The effects of sediment transport on grain-size distributions, J. Sediment. Res. **55**, 457 (1985).

[25] J. R. F. Arthur and T. Dunstan, Radiography measurements of particle packing, Nature **223**, 464 (1969).

[26] B. R. Rust, Pebble orientation in fluvial sediments, J. Sediment. Petrol. **42**, 384-388 (1972).

[27] M. E. Kauffman and D. F. Ritter, Cobble imbrication as a sensitive indicator of subtle local changes in river flow direction, Geology **9**, 299-302 (1981).

[28] I. C. Davies and R. G. Walker, Transport and deposition of resedimented conglomerates: the Cap Enragé Formation, Cambro-Ordovician, Gaspé, Quebec, J. Sediment. Petrol. **44**, 1200-1216 (1974).

[29] M. Rocheleau and J. Lajoie, Sedimentary structures in resedimented conglomerate of the Cambrian flysch, L'Islet, Quebec Appalachians, J. Sediment. Petrol. **44**, 826-836 (1974).

[30] W. E. Elston and E. I. Smith, Determination of flow direction of rhyolitic ash-flow tufts from fluidal textures, Geol. Soc. Am. Bull. **81**, 3393-3406 (1970).

[31] C. E. Johansson, Orientation of pebbles in running water: A laboratory study, Geogr. Ann. **45**, 85–112 (1963).

Microstructural differences between naturally-deposited and laboratory beach sands

SUPPLEMENTARY MATERIAL

Amy Ferrick,[1] Vanshan Wright,[2,3] Michael Manga,[1] and Nicholas Sitar[4]

[1]*University of California Berkeley, Department of Earth and Planetary Science, Berkeley, California, USA, 94720*
[2]*Woods Hole Oceanographic Institution, Geology and Geophysics Department, Woods Hole, Massachusetts, USA, 02543*
[3]*University of California San Diego, Scripps Institution of Oceanography, La Jolla, California, USA, 92037*
[4]*University of California Berkeley, Department of Civil and Environmental Engineering, Berkeley, California, USA, 94720*

I.   SAMPLE COLLECTION

For the reader's reference, we provide an image of sample collection at the Alameda County beach (Fig. S1).

FIG. S1. Sample collection.

II.   ADDITIONAL RESULTS

We quantify microstructural properties beyond those discussed in the main text. These extended results, including grain size and grain shape, are listed in Table SI. Sorting is calculated as the Inclusive Graphic Standard Deviation:

$$\sigma_I = \frac{\phi 84 - \phi 16}{4} + \frac{\phi 95 - \phi 5}{6.6},$$

where ϕ84 is the phi value of the 84th percentile of grain size distribution [1]. The phi value of a given grain diameter is calculated as

$$\phi = -\log_2 D,$$

where D is grain diameter in mm. Sphericity is calculated as

$$S = \frac{36\pi V^2}{A^3},$$

where V is grain volume and A is grain surface area [2]. Here, a sphericity of 1 is a perfect sphere.

III. EFFECT OF IMAGE RESOLUTION

We provide the graphical results of the effect of image resolution on coordination number in Fig. S2. See the main text for a description of the procedure. As image resolution increases, the number of contacts detected approaches the ground truth value.
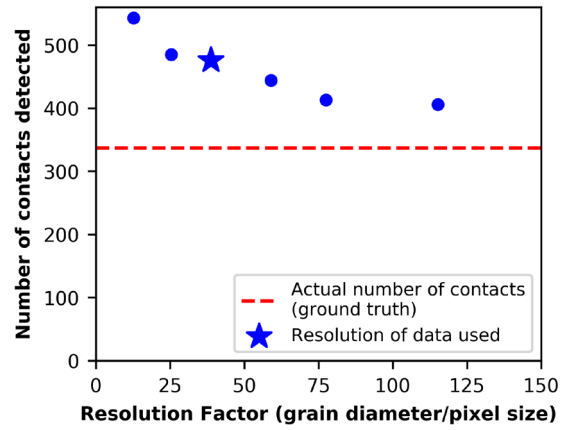
FIG. S2. Effect of image resolution on contact detection.

TABLE S1. Microstructural properties of naturally-deposited and pluviated sands.

Deposition Method	Depth (cm)	Porosity	Mean grain volume (mm³)	Mean grain surface area (mm²)	Mean grain equivalent sphere diameter (mm)	Sorting	Mean sphericity
Natural	1	0.403	0.0070	0.21	0.22	0.50	0.82
Natural	6	0.374	0.0122	0.30	0.26	0.48	0.82
Natural	11	0.371	0.0078	0.23	0.23	0.48	0.82
Pluviated	n/a	0.385	0.0051	0.16	0.19	0.55	0.83

[1] R. L. Folk and W. C. Ward, Brazos River bar [Texas]; a study in the significance of grain size parameters, J. Sediment. Res. **27**, 3-26 (1957).

[2] O. Stamati, E. Andò, E. Roubin, R. Cailletaud, M. Wiebicke, G. Pinzon, C. Couture, R. C. Hurley, R. Caulk, D. Caillerie, and T. Matsushima, spam: Software for Practical Analysis of Materials, J. Open Source Softw. **5**, 2286 (2020).